Proceedings of the ASME 2020 Conference on Smart Materials,
Adaptive Structures and Intelligent Systems
SMASIS2020
September 15, 2020, Virtual, Online

SMASIS2020-2411

ENHANCED SOUND ENERGY HARVESTING BY LEVERAGING GRADIENT-INDEX PHONONIC CRYSTALS

Ahmed Allam, Karim Sabra, Alper Erturk

Woodruff School of Mechanical Engineering, Georgia Institute of Technology, Atlanta, GA

ABSTRACT

We explore the harvesting of acoustic waves by leveraging a 3D-printed gradient-index phononic crystal (GRIN-PC) lens design. The concept is demonstrated numerically and experimentally for audio frequency range acoustic waves in air. Unit cell design procedure to achieve the required refractive index profile and numerical simulations of the band structure are executed using a high-fidelity finite-element model, followed by 3D simulations of the acoustic wave field for validation of the lens performance. Performance enhancement by focusing acoustic waves is quantified along with the level of anisotropy in the resulting 3D lens design. Additionally, a fully coupled multiphysics framework is developed to cover acoustic-structure interaction, piezoelectric coupling, as well as electrical load impedance. Finite-element simulations include the GRIN-PC lens and the harvester components along with basic electrical load to quantify the electrical power. In the full numerical simulations, design parameters such as the unit cell design, aperture of the lens, directional effects and anisotropy are explored in detail. Specifically, efforts are summarized on the unit cell design to minimize the directional sensitivity, toward making the lens close to omnidirectional.

Keywords: Piezoelectric energy harvesting, acoustics, phononic crystals

1. INTRODUCTION

Acoustic energy harvesting has received growing attention as a viable alternative for powering small electronic devices. Triboelectric [1], electromagnetic [2], and more commonly piezoelectric energy harvesters [3] have been used to convert sound into useful electric power for operating wireless sensors located in inaccessible locations. While sound waves are abundantly available in everyday life, they are characterized by a low power density. To efficiently harvest acoustic energy, it needs to be focused and localized at the energy harvester location. This localization could be achieved using several approaches. For example, Helmholtz resonators with harvesters built into their cavity walls have been proposed to localize sound with various configurations [4–7]. The acoustic energy is localized at the resonator at its resonance frequency and could be efficiently harvested to generate up to milliwatts of electric power [5]. Other forms of resonators such as tube and quarter wave resonators have been also used to harvest acoustic energy by fitting them with piezoelectric diaphragms [8,9]. Acoustic/elastic phononic crystals and metamaterials have been also suggested to enhance the performance of energy harvesters by trapping acoustic energy at the harvester location [10–13]. Phononic crystals (PCs) and locally resonant metamaterials are characterized by the presence frequency bandgaps in which acoustic or elastic waves cannot propagate. Introducing a defect in the ordered structure of these materials traps the energy at this location and allows for its extraction using an energy harvester. PCs and metamaterials have been also used to focus acoustic and elastic energy by carefully designing mirrors to reflect incident waves to a focal point where a harvester is positioned [14,15].

Gradient index phononic crystals (GRIN-PCs) were suggested to construct different types of devices to guide and focus elastic waves for energy harvesting in plates [16–18]. They are constructed by gradually varying the construction of PCs in space to vary their refractive index. Unlike geometrical lenses which require a sudden change in the refractive index (and hence the impedance) to function correctly, GRIN-PCs depend on gradual change in medium properties to guide the direction of wave propagation. This minimizes the power reflected due to impedance mismatch and allows for more power to reach the harvester increasing its performance.

GRIN-PCs have been also used to focus acoustic waves in air. Climente et al. [19] fabricated a 2D gradient index sonic crystal lens based on the hyperbolic secant profile to focus airborne sound. More recently along with advancements in 3D printing technology, Xie et al. [20] succeeded in fabricating a 2.5D and 3D Luneburg lens capable of focusing acoustic waves in air. The spherical/circular profile of Luneburg lens allows incident plane waves to be focused on the other side of the lens

regardless of their direction. This was exploited by the group to enhance the performance of ultrasonic imaging using a 2.5D lens.

We propose using a Luneburg lens profile based design to focus airborne acoustic waves at a piezoelectric harvester to enhance the harvested electrical power. In addition to its omnidirectional focusing characteristics, the spherical gradient of Luneburg lens allows for gradual impedance change in the wave propagation direction. This would minimize wave reflection and makes it a perfect candidate for enhancing the performance of the piezoelectric harvester. In this work, the PC unit cell structure and characteristics are discussed in detail highlighting the sources of anisotropy that arises from the periodicity of the PC. A 3D GRIN-PC lens is then designed simulated, 3D-printed and experimentally validated. The factors affecting the lens performance are discussed with the aim of maximizing the amplitude of the pressure waves at the focal spot. A piezoelectric harvester is then placed at the focal point of the lens and the power enhancement due to the presence of the lens is analyzed.

2. GRIN-PC LENS DESIGN

A simple cubic PC with a unit cell consisting of a 3D-printed cross-shaped polymer structure is considered (inset of Figure 1a). An acoustic finite element model (FEM) for a single PC unit cell was used to estimate the dispersion as shown in Figure 1a. Air was modelled as a periodic acoustic domain with speed of sound $c_{air} = 343$ m/s and density $\rho_{air} = 1.14$ kg/m^3. Since the impedance mismatch between the polymer and air is several orders of magnitude, it was assumed rigid, and was modelled as internal hard acoustic boundaries. The volume filling fraction of the unit cell is defined as $\phi = (3ah^2 - 2h^3)/a^3$ and represents volume of the polymer to the total volume of the cell. The effective speed of sound of the crystal $c_{eff} = 2\pi f/k$ can be controlled by changing the value of ϕ which changes of the slope of the dispersion relation as shown in Figure 1a, where f is the frequency and k is the wavenumber. The effective refractive index of the unit cell, defined as $n = c_{air}/c_{eff}$, is shown in Figure 1b. For a constant filling fraction, the effective refractive index of the material becomes more frequency dependent i.e. less broadband as the frequency increases (approaches the brag bandgap). The refractive index also becomes more frequency dependent as the filling fraction increases. A frequency of 18 kHz was selected as a design frequency for the Luneburg lens, and the effective refractive index was plotted, in Figure 1c, against the filling fraction. Figure 1c could be used to construct any GRIN-PC refractive index profile by choosing the corresponding filling fraction to the desired refractive index value. Three directions for wave propagation inside the PC are considered in Figure 1c (denoted by Miller indices). The effective refractive index at the design frequency is anisotropic (propagation direction dependent), and the degree of anisotropy is directly proportional to the filling fraction. It also depends on the target design frequency with higher anisotropy observed at higher frequencies.

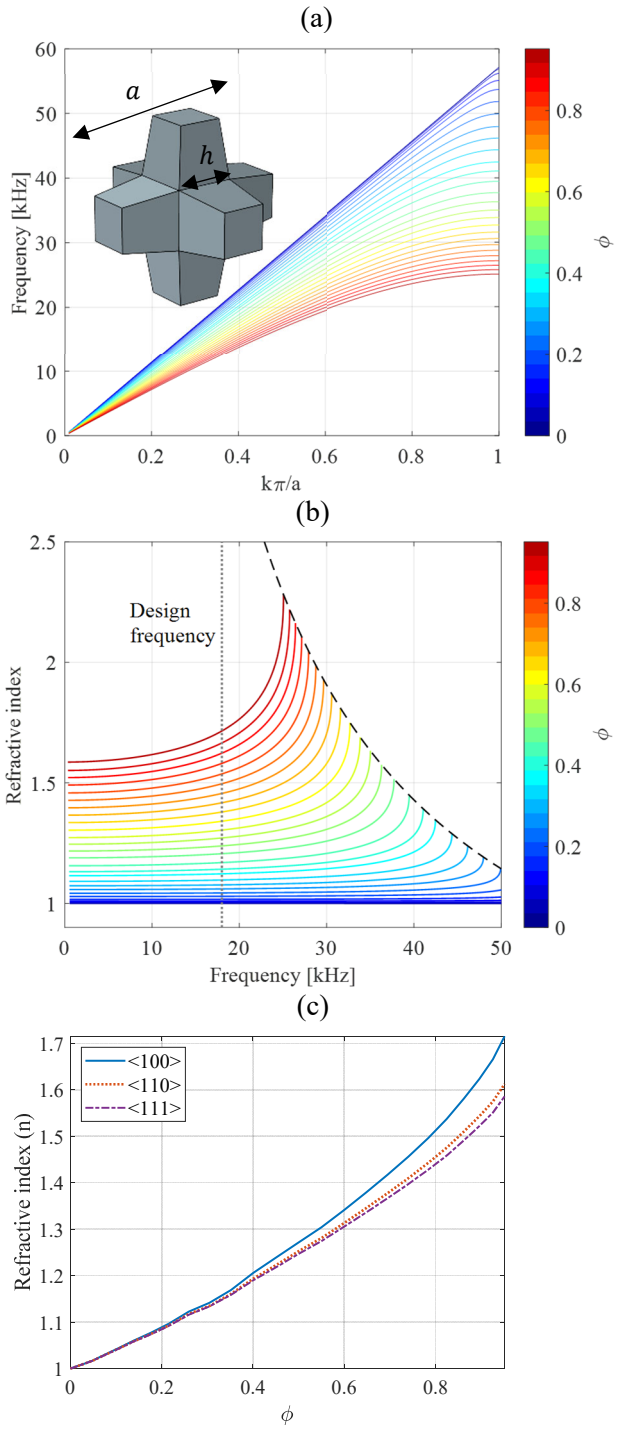

Figure 1: (a) Dispersion plot of a 3mm unit cell for different filling fraction values. (b) The effective refractive index of the PC versus frequency for different filling fraction values. (c) The effective refractive index versus the filling fraction of the cell for different wave propagation directions.

The refractive index profile in direction <100> was used to construct a GRIN-PC lens with the profile: $n(r) = \sqrt{2 - (r/R)^2}$, where r is the radial location inside the lens and R is the radius of the lens. The analytic profile was discretized for a unit cell of size $a = 3$ mm to construct lens of radius $R = 30$ mm with 10 unit cells along the radius. The analytic profile as well as the discretized refractive in the main lattice directions are shown in Figure 2a. The refractive index deviates from the analytic profile for the <110> and <111> directions which is expected to affect the performance of the lens for waves incident in these directions. This anisotropy could be reduced by operating at lower frequencies or using a smaller unit cell to implement the lens. The discretized profile was used to construct the GRIN-PC lens shown in Figure 2b by using Figure 1c to estimate the required filling fraction at each unit cell. The cross-sections of the cross-shapes were tapered to reduce the effect of discretization between each two neighboring unit cells.

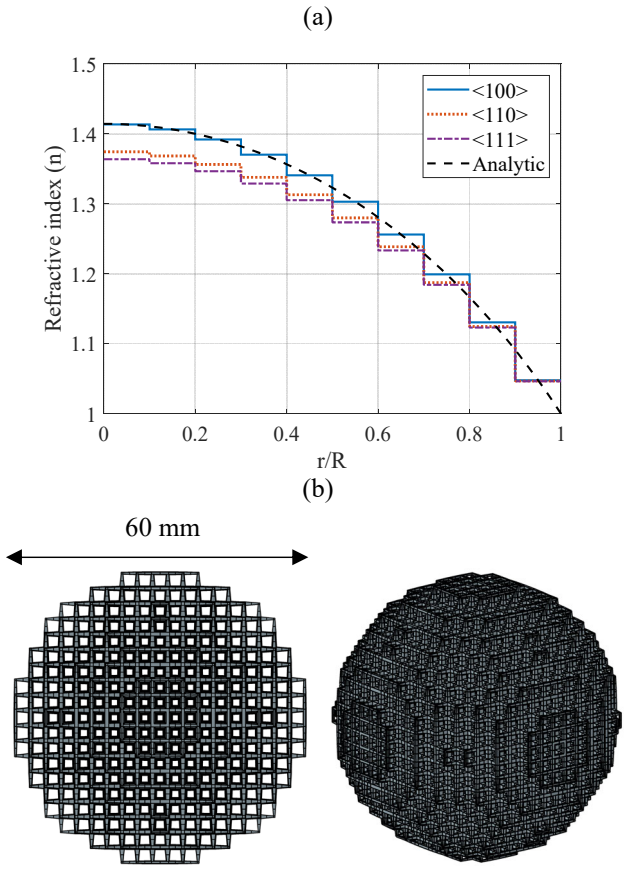

Figure 2: (a) Analytic refractive index profile of Luneburg lens vs the discretized profile used in the implementation of the GRIN-PC lens. The effective refractive index in the diagonal <110> and <111> directions are also shown. (b) Side and 3D view of the designed GRIN-PC lens based on the discretized lens profile in (a).

3. LENS DESIGN VALIDATION

The designed lens was 3D printed using Formlabs Form 2 stereolithography (SLA) 3D printer using a layer height of 100 μm and clear Formlabs resin. The printing time was approximately 6 hours.

3.1 Numerical model

A time domain FEM model was constructed to simulate incident plane waves on the lens. The lens was modeled as hard boundary to an acoustic domain discretized with 7 elements per wavelength. The lens was ensonified with a plane Gaussian pulse centered at 18 kHz with 30% bandwidth, and the acoustic domain was surrounded with radiation boundaries to minimize wave reflections. A Courant-Friedrichs-Lewy (CFL) condition of 0.2 was used to ensure accurate time stepping.

3.2 Experimental Setup

The scanning microphone setup, shown in Figure 3 was used to measure the pressure field behind the lens due to the incident plane wave. A speaker with frequency range of 40 Hz-22 kHz was excited with a Gaussian pulse centered at 18 kHz with 30% bandwidth. A 1/4" free field Larson Davis 2520 microphone was mounted on an automated XYZ stage to scan the pressure field at three perpendicular planes behind the lens. The grid cover of the microphone was removed to ensure that the pressure field could be measured as close as possible to the back surface of the lens. The microphone signal was digitized with a Handyscope HS3 oscilloscope, and a software was used to synchronize the excitation of the speaker with the data acquisition. The received signal was time gated to avoid including any wall reflections in the measurement. The pressure field was measured once with the lens present, then a second time with the lens removed to estimate the normalized pressure change due to the presence of the lens. The lens was rotated to simulate plane waves incident from a different angle and the measurement was repeated.

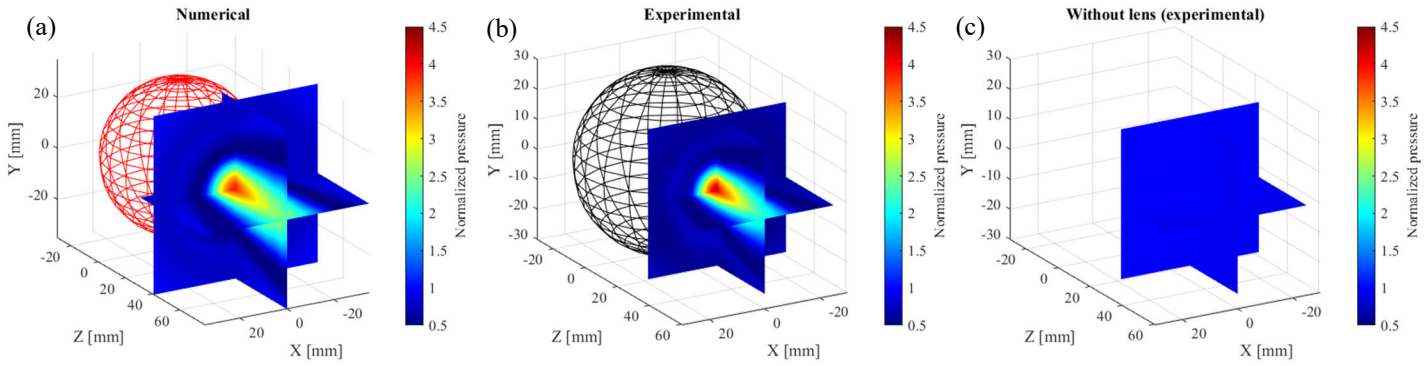

Figure 4: Peak pressure field behind the lens estimated (a) numerically and (b) experimentally. The pressure field in the absence of the lens is shown in (c) for comparison.

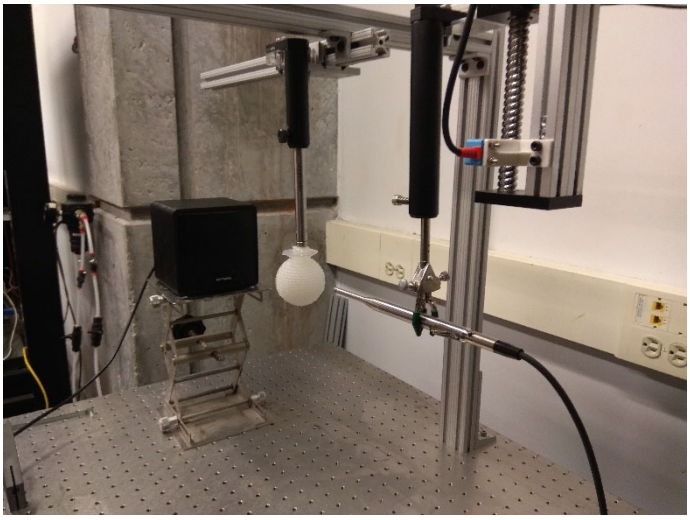

Figure 3: Setup for measuring the acoustic pressure field of the 3D-printed GRIN-PC lens.

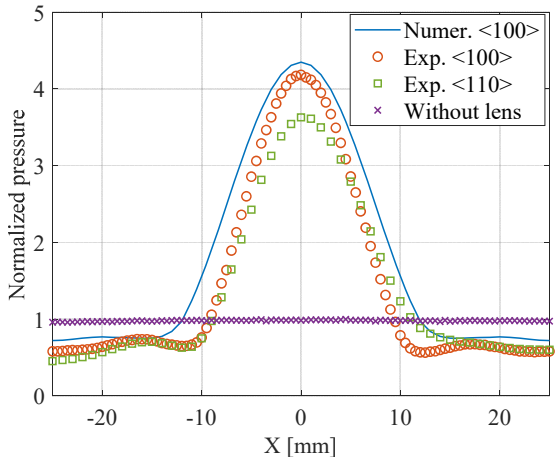

Figure 5: Normalized pressure at the focal plane obtained numerically and experimentally. The experimental pressure field is estimated for waves propagating the directions <100> and <110> with respect to the PC lattice.

3.3 Results and discussion

The peak pressure field of the lens is shown in Figure 4 at the focal spot of the lens with incident acoustic waves traveling in the positive Z direction. The experimental results are in good agreement with the numerical predictions obtained using the FEM. A clear focal spot is observed behind the lens compared to the case without the lens, and the estimated focal spot size and shape is in good agreement with the numerical predictions. The pressure field at the center of the focal plane is shown in Figure 5. The experimental results show a narrower and slightly lower amplitude at the focal spot than predicted by the finite element simulations. This is attributed to the directivity pattern and the frequency response of the speaker used which was not accounted for in the numerical model. The results for <110> wave incidence show a reduction of 15% in the peak pressure amplitude compared to the <100>. This reduction is justified by the inherent anisotropy in the PC used to design the lens as shown in Figure 2a.

Figure 6 shows the experimental pressure time series at the focal point of the lens compared to the baseline case where the lens is not present. A pressure gain of 4.2 was observed in both the peak and RMS pressure at the focal point. This corresponds to an increase in acoustic intensity at the focal spot by a factor of 17.52 around the target design frequency of 18 kHz. The effect of changing the center frequency of the excitation was studied experimentally as shown in Figure 7. As the frequency of the incident pulse increases, the full width at half maximum (FWHM) decreases which is expected since the diffraction limit decreases with increased frequency allowing for the power to be focused at a smaller spot.

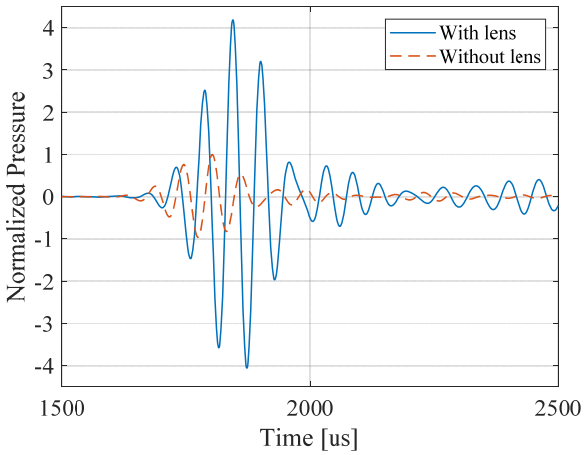

Figure 6: Time series for the normalized pressure field measured at the focal point of the lens. The pressure field at the same location in the absence of the lens is shown for reference.

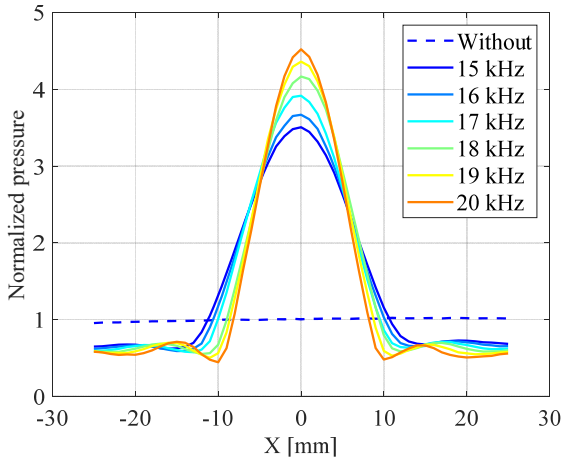

Figure 7: Normalized peak pressure at the focal plane obtained experimentally for different center frequencies. The bandwidth was kept constant at 6 kHz.

4 ENERGY HARVESTING PERFORMANCE ENHANCEMENT

To demonstrate the ability of the GRIN-PC lens to enhance the performance of sound energy harvesting, a piezoelectric energy harvester was placed at the focal spot of the lens as shown in Figure 8. The harvester is a circular unimorph with outer diameter of 13.5 mm. It consists of a substrate layer of thickness 0.2 mm made of stainless steel and a piezoelectric layer of thickness 0.15 mm made of modified PZT-4. A variable load resistor was connected to the harvester via two thin wires which were also used to suspend the harvester to emulate free boundary conditions on its edges.

A frequency domain piezoelectric FEM was constructed to predict the behavior of the harvester and tune its performance. An axisymmetric FEM of the harvester was subjected to a uniform harmonic pressure of 10 Pa and the output power across different resistor values was estimated as shown in Figure 9. Two power peaks at 14.5 kHz and 15.5 kHz are observed representing the short and open-circuit resonance frequencies of the harvester. The output power is larger for resistance values closer to the open-cricuit resonace (around 50 kΩ); however, their frequency bandwidth is narrowrer compared resistor values between 1 kΩ and 10 kΩ representing the optimum resistance range.

A time-dependent fully coupled piezoelectric- acoustic FEM was also developed to predict the performance of the lens-harvester system. Incident acoustic plane waves in air were used to excite the system and the output voltage signal across different resistance values was evaluated. For each resistor value, the harvester was excited with and without the presence of the lens to characterize the performance enhancement.

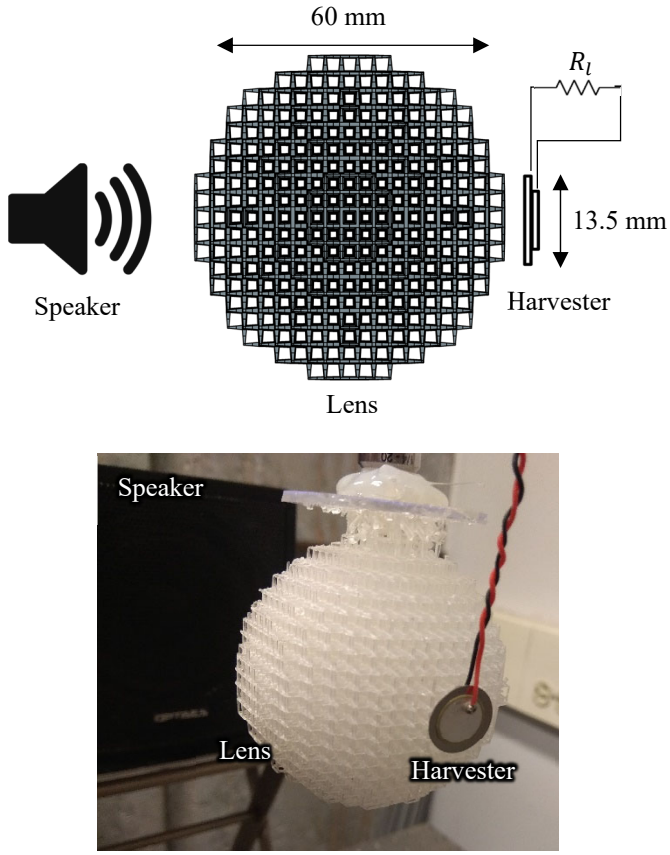

Figure 8: Layout of the experimental setup used to estimate the output power enhancement of a piezoelectric energy harvester placed at the focal spot of the developed GRIN-PC lens.

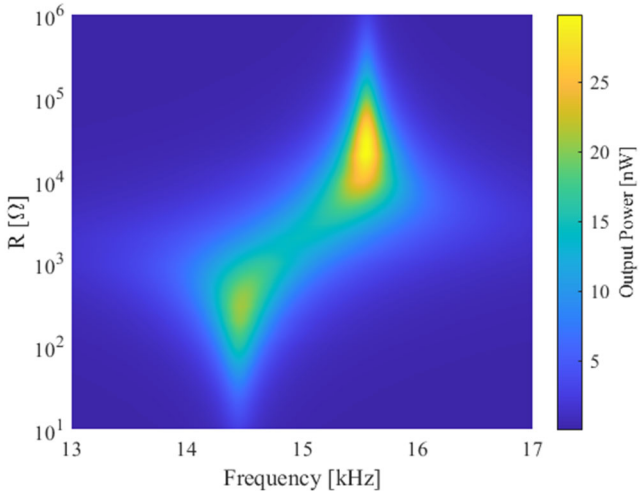

Figure 9: Output power of the harvester when subjected to a uniform harmonic pressure of 10 Pa. The power is plotted vs excitation frequency and load resistance.

In the experimental setup shown in Figure 8, the lens-harvester system was excited with a 15 kHz modulated Gaussian pulse with a bandwidth of 4 kHz generated through the loud speaker. The amplitude of the incident acoustic plane wave at the harvester location was 7 Pa (measured in the absence of the lens and harvester). The voltage generated across the load resistor was measured and used to estimate the output power of the harvester at different resistance values. The lens was then removed and the output power of the harvester was measured again as a baseline to estimate the power enhancement due to the presence of the lens.

The voltage time series for different resistor values are shown in Figure 10. Experimental and numerical results are in good agreement despite the presence of measurement noise. The noise becomes more significant for low resistance values (Figure 10e) since both the output voltage and power drop. The voltage response is less damped for both small and large resistance values (Figure 10a&d). The slow decay of the response at these resistance values indicates a suboptimal performance since energy is not efficiently dissipated by the resistors. For close to optimal resistance values (Figure 10b&c), the signal decay is faster indicating a stronger coupling between the mechanical and electrical domains.

For all the resistor values considered in Figure 10 the harvested pulse was much longer than the 0.5 ms incident acoustic pulse. This is attributed to the narrow bandwidth of the harvester compared to the incident pulse. The bandwidth of the harvester is limited to a maximum of 1 kHz, while the incident pulse had a bandwidth of 4 kHz. The presence and absence of the lens had almost no effect on the width of the pulse for all the resistors values which shows that the bandwidth of the lens is much larger than that of the harvester. The output power of the system could thus be further enhanced by using a harvester of larger bandwidth.

The peak power generated for different resistor values is shown in Figure 11. The generated power is maximized when an optimal resistance value within 1-10 kΩ is connected to the harvester. The presence of the lens enhanced the output power by up to an order of magnitude for all resistor values. The electric power gain is slightly lower than the pressure power gain that can be achieved by the lens at the considered center frequency (15 kHz), see in Figure 7, which is expected since the dimensions of the harvester are larger than the focal spot of the lens.

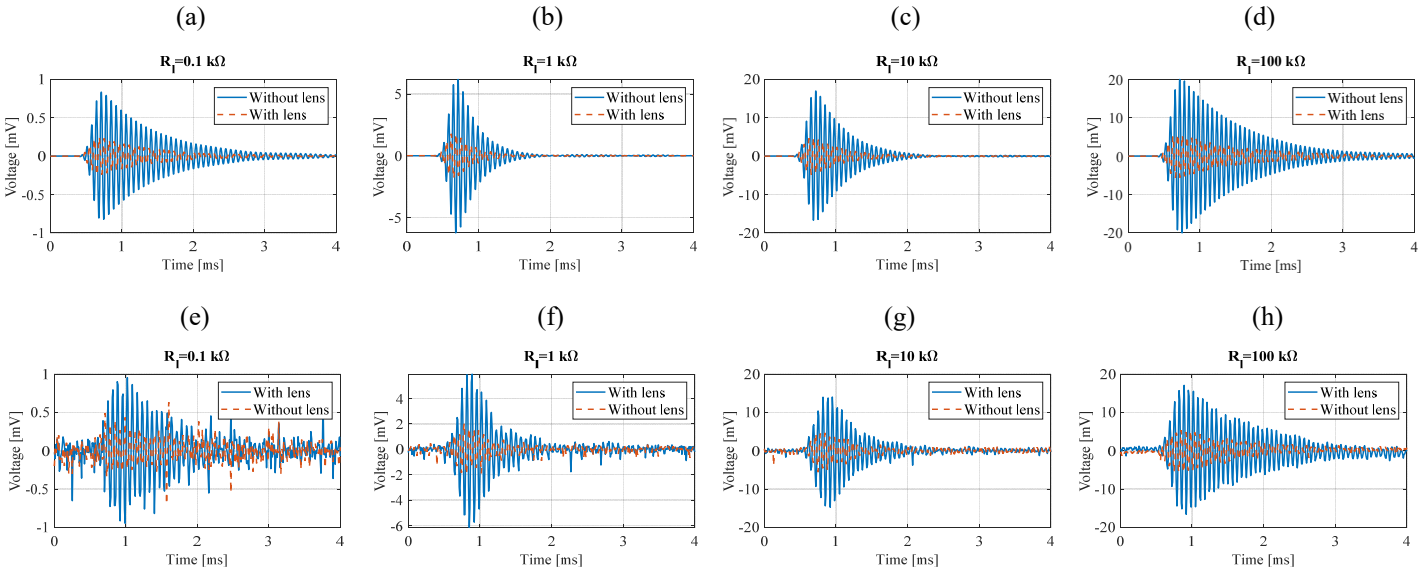

Figure 10: Harvester voltage time series estimated numerically (a-d) and experimentally (e-h) for different resistance values. For each case the voltage generated with and without the presence of the lens is shown.

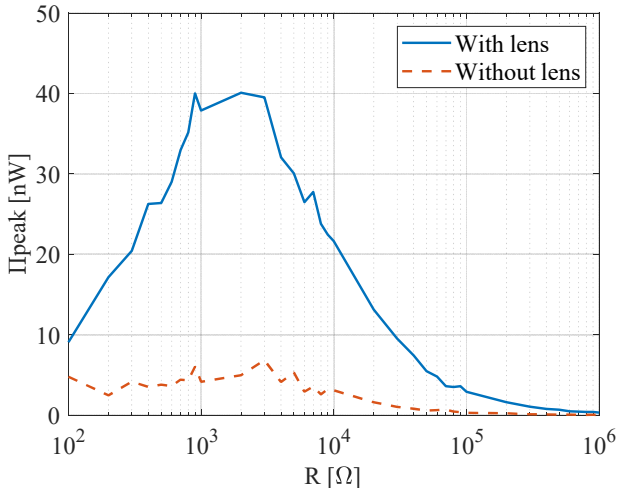

Figure 11: Peak harvested electrical power versus load resistance for an incident acoustic plane wave of amplitude 7 Pa on the lens-harvester system. The baseline case for the harvester without the lens is also shown.

5 CONCLUSION

A 3D-printed GRIN-PC lens based on Luneburg lens profile was designed, simulated and experimentally tested to focus acoustic waves in air. The lens was capable of achieving a peak power gain of 23.5 compared to the free field of without the lens. The lens was tested over a broad frequency range starting from 15 kHz up to 24 kHz with variation in performance limited by the diffraction limit at each frequency. The output power of a piezoelectric energy harvester placed at the focal point of the lens was significantly increased for compared to the baseline case verifying that the lens could be used for enhancing energy harvesting performance in a broadband sense. Due to the omnidirectional focusing characteristics of the developed lens, multiple harvesters might be placed around the lens to harvest acoustic energy incident from different directions further enhancing the power output of the devices.

ACKNOWLEDGEMENTS

This work was supported by the National Science Foundation CMMI grant 1727951.

REFERENCES

[1] Fan, X., Chen, J., Yang, J., Bai, P., Li, Z., and Wang, Z. L., 2015, "Ultrathin, Rollable, Paper-Based Triboelectric Nanogenerator for Acoustic Energy Harvesting and Self-Powered Sound Recording," ACS Nano, **9**(4), pp. 4236–4243.

[2] Izhar, and Khan, F. U., 2018, "Electromagnetic Based Acoustic Energy Harvester for Low Power Wireless Autonomous Sensor Applications," Sens. Rev., **38**(3), pp. 298–310.

[3] Khan, F. U., and Izhar, 2015, "State of the Art in Acoustic Energy Harvesting," J. Micromechanics Microengineering, **25**(2), p. 023001.

[4] Horowitz, S. B., Sheplak, M., Cattafesta, L. N., and Nishida, T., 2006, "A MEMS Acoustic Energy Harvester," J. Micromechanics Microengineering, **16**(9), pp. S174–S181.

[5] Liu, F., Phipps, A., Horowitz, S., Ngo, K., Cattafesta, L., Nishida, T., and Sheplak, M., 2008, "Acoustic Energy Harvesting Using an Electromechanical Helmholtz Resonator," J. Acoust. Soc. Am., **123**(4), pp. 1983–1990.

[6] Yuan, M., Cao, Z., Luo, J., Zhang, J., and Chang, C., 2017, "An Efficient Low-Frequency Acoustic Energy Harvester," Sens. Actuators Phys., **264**, pp. 84–89.

[7] Liu, G.-S., Peng, Y.-Y., Liu, M.-H., Zou, X.-Y., and Cheng, J.-C., 2018, "Broadband Acoustic Energy Harvesting Metasurface with Coupled Helmholtz Resonators," Appl. Phys. Lett., **113**(15), p. 153503.

[8] Li, B., You, J. H., and Kim, Y.-J., 2013, "Low Frequency Acoustic Energy Harvesting Using PZT Piezoelectric Plates in a Straight Tube Resonator," Smart Mater. Struct., **22**(5), p. 055013.

[9] Guo, H., Wang, Y., Wang, X., and Xu, C., 2018, "Investigation on Acoustic Energy Harvesting Based on Quarter-Wavelength Resonator Phononic Crystals," Adv. Mech. Eng., **10**(1), p. 1687814017748077.

[10] Wu, L.-Y., Chen, L.-W., and Liu, C.-M., 2009, "Acoustic Energy Harvesting Using Resonant Cavity of a Sonic Crystal," Appl. Phys. Lett., **95**(1), p. 013506.

[11] Wang, W.-C., Wu, L.-Y., Chen, L.-W., and Liu, C.-M., 2010, "Acoustic Energy Harvesting by Piezoelectric Curved Beams in the Cavity of a Sonic Crystal," Smart Mater. Struct., **19**(4), p. 045016.

[12] Carrara, M., Cacan, M. R., Toussaint, J., Leamy, M. J., Ruzzene, M., and Erturk, A., 2013, "Metamaterial-Inspired Structures and Concepts for Elastoacoustic Wave Energy Harvesting," Smart Mater. Struct., **22**(6), p. 065004.

[13] Yang, A., Li, P., Wen, Y., Lu, C., Peng, X., Zhang, J., and He, W., 2013, "Enhanced Acoustic Energy Harvesting Using Coupled Resonance Structure of Sonic Crystal and Helmholtz Resonator," Appl. Phys. Express, **6**(12), p. 127101.

[14] Carrara, M., Cacan, M. R., Leamy, M. J., Ruzzene, M., and Erturk, A., 2012, "Dramatic Enhancement of Structure-Borne Wave Energy Harvesting Using an Elliptical Acoustic Mirror," Appl. Phys. Lett., **100**(20), p. 204105.

[15] Qi, S., and Assouar, B., 2017, "Acoustic Energy Harvesting Based on Multilateral Metasurfaces," Appl. Phys. Lett., **111**(24), p. 243506.

[16] Tol, S., Degertekin, F. L., and Erturk, A., 2016, "Gradient-Index Phononic Crystal Lens-Based Enhancement of Elastic Wave Energy Harvesting," Appl. Phys. Lett., **109**(6), p. 063902.

[17] Tol, S., Degertekin, F. L., and Erturk, A., 2017, "Phononic Crystal Luneburg Lens for Omnidirectional Elastic Wave

Focusing and Energy Harvesting," Appl. Phys. Lett., **111**(1), p. 013503.
[18] Tol, S., Degertekin, F. L., and Erturk, A., 2019, "3D-Printed Phononic Crystal Lens for Elastic Wave Focusing and Energy Harvesting," Addit. Manuf., **29**, p. 100780.
[19] Climente, A., Torrent, D., and Sánchez-Dehesa, J., 2010, "Sound Focusing by Gradient Index Sonic Lenses," Appl. Phys. Lett., **97**(10), p. 104103.
[20] Xie, Y., Fu, Y., Jia, Z., Li, J., Shen, C., Xu, Y., Chen, H., and Cummer, S. A., 2018, "Acoustic Imaging with Metamaterial Luneburg Lenses," Sci. Rep., **8**(1), p. 16188.